Journal: Remote Sensing of the Environment

Title: Statistical correction of lidar-derived digital elevation models with multispectral airborne imagery in tidal marshes

Kevin J. Buffington[a,b,*], Bruce D. Dugger[a], Karen M. Thorne[b], John Y. Takekawa[b],

[a] Department of Fisheries and Wildlife, Oregon State University, Corvallis, OR 97331
[b]US Geological Survey, 505 Azuar Dr., Vallejo, CA 94592

*Corresponding author at 104 Nash Hall, Oregon State University, Corvallis, OR 97331
Email addresses: kevin.buffington@oregonstate.edu (K. Buffington), bruce.dugger@oregonstate.edu (B. Dugger), kthorne@usgs.gov (K. Thorne), john.takekawa@usgs.gov (J. Takekawa)

Abstract

Airborne light detection and ranging (lidar) is a valuable tool for collecting large amounts of elevation data across large areas; however, the limited ability to penetrate dense vegetation with lidar hinders its usefulness for measuring tidal marsh platforms. Methods to correct lidar elevation data are available, but a reliable method that requires limited field work and maintains spatial resolution is lacking. We present a novel method, the Lidar Elevation Adjustment with NDVI (LEAN), to correct lidar digital elevation models (DEMs) with vegetation indices from freely available multispectral airborne imagery (NAIP) and RTK-GPS surveys. Using 17 study sites along the Pacific coast of the U.S., we achieved an average root mean squared error

(RMSE) of 0.072 m, with a 40-75% improvement in accuracy from the lidar bare earth DEM. Results from our method compared favorably with results from three other methods (minimum-bin gridding, mean error correction, and vegetation correction factors), and a power analysis applying our extensive RTK-GPS dataset showed that on average 118 points were necessary to calibrate a site-specific correction model for tidal marshes along the Pacific coast. By using freely available data and with minimal field surveys, we showed that lidar-derived DEMs can be adjusted for greater accuracy while maintaining high (1 m) resolution.

Keywords: RTK-GPS surveys, accuracy, LEAN, Normalized Difference Vegetation Index (NDVI), sea-level rise

Introduction

The structure and function of tidal marshes are strongly driven by physical gradients including elevation and tidal range. Elevation, relative to mean sea level, is responsible for variation in abiotic features like accretion rates (Butzeck et al., 2014), soil characteristics (Cahoon and Reed, 1995), pore water salinity, and oxygen availability (Hackney et al., 1996). Tidal marsh plants and animals have numerous adaptations for surviving these gradients in physical conditions (Pennings et al., 1992; Silvestri et al., 2005); however, the elevation range in which species can persist is often narrow (< 1 m). In addition, small changes in marsh elevation can lead to large increases in inundation time under normal tidal cycles. Consequently, accurate characterization of elevation is critical for understanding tidal marsh ecogeomorphology, and tidal marsh structure and function are especially sensitive to changes in relative elevation due to sea level rise (Kirwan and Temmerman, 2009; Kolker et al., 2009).

Growing concern about the effects of climate change and sea-level rise on tidal marsh sustainability has increased interest in creating accurate digital elevation models (DEMs) of tidal marshes to better inform modeling and planning efforts. Airborne light detection and ranging (lidar) is a common tool used to generate DEMs and is becoming more readily available to coastal managers and scientists. High point return densities (1-10 points/m) and relative ease of data collection across large areas have made lidar a popular option for measuring bare earth elevation and vegetation height (Hodgson and Bresnahan, 2004; Kane et al., 2010). In areas with low vegetative cover (e.g., open terrain or concrete), the vertical accuracy of airborne lidar is between 15-25 cm root mean squared error (RMSE, eq. 2; Hodgson and Bresnahan 2004, Mitasova et al. 2009), with normally distributed errors (mean error approaching zero). However, the inability of the laser pulse to penetrate the dense vegetation canopy of most tidal marshes limits the accuracy of lidar-derived DEMs (Montané and Torres, 2006; Rosso et al., 2005; Sadro et al., 2007; Schmid et al., 2011; Hladik and Alber, 2012). For example, one study found that just 3% of lidar points were reflected off the marsh surface (Sadro et al., 2007), and another found that error in tidal marshes was greater than in adjacent upland habitats (Schmid et al., 2011), creating a positive bias in mean elevation of 10-40 cm (Sadro et al., 2007; Foxgrover et al., 2011; Hladik and Alber, 2012). Even lidar collected during periods of seasonally low biomass in tidal marshes can exhibit significant (>20 cm) vertical errors (Schmid et al., 2011). Correcting vertical errors is necessary for accurate predictions of flooding risk, marsh elevation change under sea-level rise, or any application where inundation is of primary concern.

Several methods have been used to correct lidar error in tidal marshes, including vegetation correction factors (Hladik and Alber, 2012), minimum-bin gridding (Schmid et al., 2011), an aboveground biomass model (Medieros et al., 2015), and statistical correction of full waveform lidar (Parrish et al., 2014); however, each of these methods have limitations that may hinder broad adoption. Vegetation correction factors require extensive vegetation surveys or expert knowledge of a marsh coupled with high accuracy GPS surveys to correlate lidar error with plant communities (Hladik and Alber 2012; overall RMSE = 0.1 m). Hyperspectral data can be useful in species and community classification in wetlands (Rosso et al., 2005; Sadro et al., 2007; Adam et al., 2010), but those data are not widely available and expensive to acquire. In addition, plant height and cover can vary substantially across elevation and salinity gradients, potentially requiring multiple corrections for a single species or community. Minimum-bin gridding (MBG) uses the minimum lidar return value within a predefined grid pixel to set the value for the DEM; as pixel size increases lidar error generally decreases as more low values are included; however, horizontal resolution of the DEM decreases and because so few lidar returns hit the marsh platform, a positive bias remains (Schmid et al. 2011; RMSE = 0.17 m). Medieros et al. (2015) used a combination of remote sensing datasets (ASTER imagery and interferometric synthetic aperture radar, InSAR) in a Florida tidal marsh to model aboveground biomass density and then correct lidar error. They achieved a 38% reduction in RMSE at 5-m horizontal resolution (0.65 to 0.40 RMSE). In addition to Real-Time Kinematic (RTK) GPS surveys, the biomass model requires labor-intensive vegetation sampling that may require destructive sampling if allometric equations for biomass are not available. Relying on two statistical models, each with a measure of uncertainty, may also limit the accuracy of the adjusted DEM. Vertical correction of full waveform lidar using waveform features is promising (Parrish et al., 2014), however, broad collection of waveform lidar is still relatively rare and it requires extensive processing skills; we focus our analysis on DEMs derived from discrete return lidar.

Our objective was to develop a correction model for lidar-derived DEMs using readily available, high resolution (1 m), multispectral (red, green, blue, near-infrared) airborne imagery from the US Department of Agriculture (USDA) National Agriculture Inventory Program (NAIP). Derived products from the NAIP imagery, such as the Normalized Difference Vegetation Index (NDVI), correlate well with the spatial variation in vegetation biomass and structure (Gamon et al., 1995; Myneni et al., 1995; Filella et al. 2004; Pettorelli et al. 2005), and we tested the ability of NDVI to calibrate a statistical model of lidar error when used in conjunction with baseline elevation datasets (e.g., RTK-GPS surveys). We developed a statistical model of lidar error for a gradient of study sites in 17 tidal marsh sites along the Pacific coast. We applied the models and compared them to RTK-GPS field data to assess DEM accuracy, and we compared the performance of our model against other commonly applied correction techniques. Finally, we determined the minimum density of RTK-GPS data points necessary to achieve a DEM with maximum accuracy and tested the sensitivity of the statistical model to use NAIP images from years different than when the lidar data were collected.

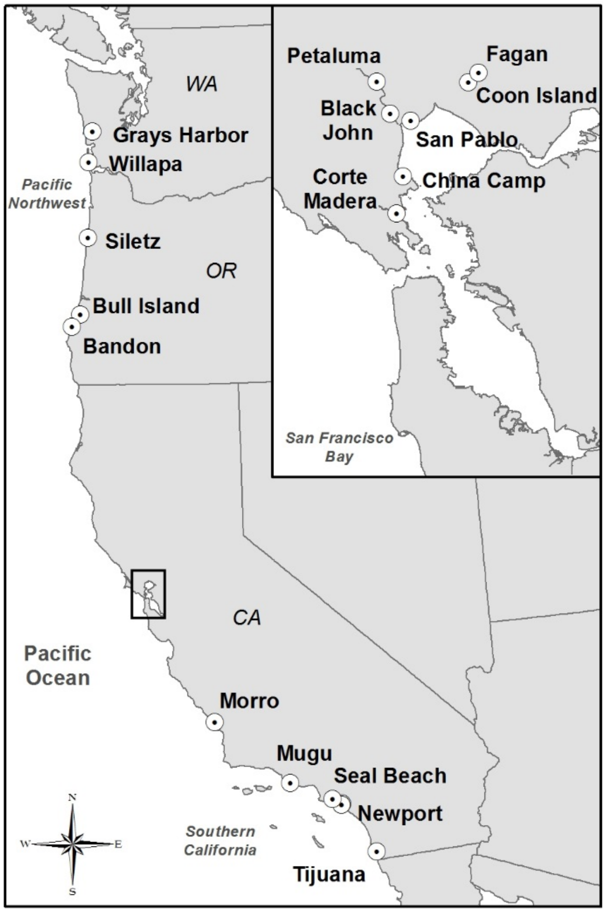

Fig. 1. Location of 17 tidal marsh study sites along the Pacific coast of the United States. Study sites represented a range of dominant tidal marsh vegetation, climate, and tidal ranges to test the applicability of model corrections across different vegetation types.

2. Methods

2.1. Study Area

Our study included 17 tidal marsh sites located in eleven estuaries where both lidar data and NAIP imagery were available (Fig. 1, Table 1). Sites were chosen to be representative of historic marsh conditions and many were on U.S. Fish and Wildlife Service National Wildlife

Refuges (NWRs). While each study site had unique ecological and geomorphic characteristics, for broad comparisons they were grouped into three regions. Pacific Northwest (PNW) sites included: Grays Harbor NWR (hereafter Grays Harbor); Tarlet Slough in Willapa Bay NWR (Willapa); Millport Slough in Siletz Bay NWR (Siletz); Bull Island within the South Slough National Estuarine Research Reserve in Coos Bay (Bull Island); and the Bandon marsh unit in Bandon NWR in the Coquille Estuary (Bandon). San Francisco Bay (SFB) sites included: Black John marsh (Black John) and Petaluma marsh (Petaluma) on the west shore of the Petaluma River at the northwest corner of San Pablo Bay; Coon Island and Fagan along the Napa river; San Pablo NWR (San Pablo) along the north shore of San Pablo Bay; China Camp State Park along the south shore of San Pablo Bay (China Camp); and the Corte Madera Marsh Ecological Reserve (Corte Madera) on the west shore of Central San Francisco Bay. Southern California (SCA) sites included: Morro Bay State Park (Morro); Naval Air Station Point Mugu (Mugu); Seal Beach NWR (Seal Beach); Upper Newport Bay Nature Preserve (Newport); and Tijuana Slough NWR (Tijuana). Tidal range increases with latitude, ranging from 1.75 m at Tijuana in the south, to 2.79 m at Grays Harbor in the north (tidesandcurrents.noaa.gov).

Table 1. Characteristics of study sites used to correct lidar data for coastal tidal marshes using NAIP imagery. Area (ha), number of RTK-GPS points and year collected, lidar and NAIP acquisition months, and dominant vegetation. More specific acquisition dates could not be determined from available metadata at Bull Island and Bandon, and we could only determine a range of dates for San Francisco Bay. Species are listed if they were found in at least 25% of vegetation survey plots (Takekawa et al., 2013, Thorne et al., 2015, Thorne et al., 2016).

Site	Area (ha)	RTK-GPS (n)	RTK Year	Lidar Acq.	NAIP Acq.	Dominant Vegetation
Pacific Northwest						
Grays Harbor	68	1166	2012	9/2009	9/2009	CarLyn, ArgSto, TriMar, PotAns
Willapa	27	420	2012	9/2009	9/2009	DisSpi, SalPac, TriMar, DesCep, CarLyn
Siletz	69	1113	2014	9/2009	6/2009	ArgSto, CarLyn, DisSpi, PotAns, JunBal
Bull Island	97	1166	2012	2008	6/2009	CarLyn, SalPac, DisSpi, DesCep
Bandon	97	1495	2012	2008	6/2009	SalPac, DisSpi, DesCep, CarLyn, AgrSto

San Francisco Bay						
Petaluma	81	623	2009	2-4/2010	6/2010	SalPac, SpaFol
Black John	31	203	2009	2-4/2010	6/2010	SalPac, SpaFol
San Pablo	147	374	2009	2-4/2010	6/2010	SalPac, SpaFol
Fagan	68	578	2010	2-4/2010	5/2010	SalPac, BolMar, PotAns
Coon Island	99	728	2009	2-4/2010	5/2010	SalPac, BolMar
China Camp	97	697	2009	2-4/2010	5/2012	SalPac, SpaFol
Corte Madera	45	399	2010	2-4/2010	5/2012	SalPac, SpaFol
Southern California						
Morro	154	2247	2013	10/2009	6/2009	SalPac, JauCar
Mugu	109	1465	2013	11/2009	6/2009	SalPac, FraSal
Seal Beach	266	3208	2011	9/2009	6/2009	SalPac FraSal, SpaFol
Newport	60	962	2012	9/2009	6/2009	SalPac, SpaFol, BatMar
Tijuana	62	896	2011	11/2009	6/2009	SalPac, JauCar, FraSal, DisSpi

Species codes are: CarLyn = *Carex lyngbyei*; ArgSto = *Agrostis stolonifera;* TriMar = *Triglochin maritima*; PotAns = *Potentilla anserine*; DisSpi = *Distichlis spicata*; DesCep = *Deschampsia cespitosa*; JunBal = *Juncus balticus*; SalPac = *Salicornia pacifica*; SpaFol = *Spartina foliosa*; JauCar = *Jaumea carnosa*; FraSal = *Frankenia salina*; BatMar = *Batis maritima*; BolMar = *Bolboschoenus maritimus*.

Plant community composition and species richness varies substantially in marshes along the Pacific coast (Table 1). The PNW sites are comparatively species rich with a mix of salt, brackish, and fresh water sedges, grasses and rushes (Thorne et al., 2015). In SFB, the higher salinity sites (San Pablo, China Camp, Corte Madera, Black John and Petaluma) are dominated by *Salicornia pacifica* (mean height 20 cm), that creates dense mats at mid-high elevations, with *Schoenoplectus spp.* (mean height 86 cm) and *Spartina foliosa* and invasive *Spartina alterniflora* hybrids (mean height 91 cm) in lower elevations and along channels. The more brackish sites (Coon Island and Fagan) have higher species richness, with *Schoenoplectus spp.*, *Typha angustifolia* (mean height 108 cm), and *Potentilla anserina* (mean height 26 cm) also common (Takekawa et al., 2013). The SCA sites are characterized by high salinity and plants with a shorter growth forms including *Salicornia pacifica* (mean height 33 cm), *Batis maritima* (mean height 20 cm), and *Distichlis spicata* (mean height 14 cm; Thorne et al., 2016).

2.2. RTK-GPS surveys

We conducted elevation surveys using survey-grade GPS rovers (RTK GPS, 2-5 cm vertical accuracy, Leica Viva GS15 and Leica GX1230, Atlanta, GA, USA) and referenced the rovers to nearby National Geodetic Survey (NGS) benchmarks. Real-time corrections were provided by the Leica SmartNet station network in SFB, while in Oregon the Oregon Real-Time GNSS Network (ORGN) provided corrections. In SCA and Washington, we deployed a Leica GS10 base station with a radio link at a temporary benchmark that provided real-time corrections to the Leica Viva GS15 rover. We surveyed nearby NGS benchmarks for vertical control. We submitted the temporary benchmark locations to the NGS Online Positioning User Service that uses the precise ephemeris from the GPS satellite network to provide accurate (< 2 cm) temporary benchmark locations. We surveyed elevations at stations placed on gridded transects that ran perpendicular to the marsh-mudflat boundary. Transects were separated by 50 m and RTK sample stations were located every 25 m (SFB) or 12.5 m (PNW and SCA) on each transect for a density of **7-**14 points per hectare. We used the geoid09 gravitational model to convert ellipsoid heights to North American Vertical Datum of 1988 (NAVD88) for the SFB and SCA sites, and used the geoid03 model for the PNW sites, matching the geoid models used in each lidar datasets. Across all sites the mean RMSE of the RTK–GPS surveys was 0.046 m.

For this study, we were interested in correcting the positive bias across the marsh platform and not in correcting possible bias in unvegetated marsh channels or mudflats. The RTK-GPS dataset used in this study were originally meant for developing DEMs through interpolation and included points that were near topographically steep features (channels and scarps). We manually removed RTK-GPS points from the dataset that were within 2 pixels (m) of marsh channels or platform edge and likely subject to error due to pixel resolution (i.e., the lidar DEM pixel represented the side or bottom of a steep channel while the RTK-GPS point is on the marsh platform adjacent to the channel).

2.3. Airborne lidar data

We obtained lidar-derived DEMs from the NOAA Digital Coastal Data Access Viewer (https://coast.noaa.gov/dataviewer/; Table 2). We used the local UTM (zone 10 or 11) for the horizontal datum, and NAVD88 for the vertical datum. We selected mean grid averaging of all lidar returns at 1 m resolution. Our goal was to use 'as-received' lidar DEMs to eliminate any lidar processing from the workflow and to maximize the accessibility of the procedure. We determined lidar elevation at each RTK-GPS location with the 'extract' function in the 'raster' package in R (www.r-project.org).

Table 2. Flight characteristics and accuracy of lidar data.

	San Francisco Bay	CA State Coastal Conservancy	DOGAMI
Contractor	Fugro EarthData	Fugro EarthData	Watershed Sciences
Sensor	Leica ALS60 MPiA	Leica ALS60 MPiA	Leica ALS50 Phase II
Points/m	1	1	8.60
RMSE (m, open terrain)	0.026	0.048	0.044
Geoid Model	Geoid09	Geoid09	Geoid03
Flightline overlap (%)	20	20	50
Altitude (m)	2000	1900	900
Field of View (degrees)	30	30	28
Pulse Rate (Hz)	121,300	121,300	105,000
Scan Rate (Hz)	41	41	52.2
Returns	Discrete	Discrete	Discrete
Abbreviation	SFB	SCA	PNW

2.3. Multispectral imagery

We obtained multispectral airborne imagery data for each site from the National Agriculture Imagery Program (NAIP, 1 m resolution; USDA Farm Service Agency). NAIP imagery is collected for each state on a rotating basis, roughly every two years and typically at the peak of the growing season. We preferentially chose imagery that was collected during the same year that lidar was flown to minimize potential error due to annual variation in plant productivity (Table 1). While the majority of our sites had imagery and lidar data collected in the same year, there were three exceptions. At two sites (Bandon, Bull Island) imagery was not available for 2008, so we used 2009 imagery instead. At China Camp and Corte Madera part of the 2010 image for the marsh was taken at high tide resulting in an uneven image; we instead used 2012 imagery for China Camp and Corte Madera. To assess the quality of georeferencing of the NAIP imagery, we visually compared NAIP and lidar landscape features (channels, roads, buildings) at each site. We found the 2009 and 2010 NAIP images aligned with the lidar and made no adjustments. The 2011 and 2012 NAIP imagery, however, were misaligned with the lidar; in ArcGis we shifted those NAIP datasets slightly (< 3 m) to align with the lidar datasets, using 1-2 points across the marsh as ground control**.**

The USDA releases full county, color-corrected mosaics of their NAIP imagery; however, the near-infrared band is removed and image compression reduces image fidelity. We instead used multiple unadjusted 4-band quarter quads at each study site for full coverage. We mosaicked together quarter quads in ENVI (v. 5, Exelis Inc, Boulder, CO, USA) using histogram matching of overlapping scenes to correct for differences in brightness across images. We then applied a dark object subtraction using the histogram of each band to correct for atmospheric interference (Chavez, 1988). From the NAIP imagery, we calculated the Normalized Difference Vegetation Index (NDVI), as:

$$\mathbf{NDVI} = \frac{\mathbf{NIR-R}}{\mathbf{NIR+R}} \qquad \text{Eq. 1.}$$

where, *NIR* is the near-infrared band (750 nm, band 4), and *R* is the red band (650 nm, band 3). NDVI is a relative index that ranges from -1 to 1, with values above 0 generally considered to be vegetated. While not an issue at our study sites, NDVI can saturate at high values; in areas where this occurs we suggest using the Wide Dynamic Range Vegetation Index instead. NDVI is also sensitive to electromagnetic absorption from water, thus it is important to use imagery collected during low tides.

2.4. Accuracy Assessment

Following the accuracy assessment guidelines from Maune et al. (2007) and the National Standard for Spatial Data Accuracy (Federal Geographic Data Committee, 1998), we used root mean squared error (RMSE), Fundamental Vertical Accuracy (FVA), and the 95th Percentile Error (PE) as metrics of DEM accuracy (Flood, 2004). RMSE is calculated as:

$$\mathbf{RMSE} = \mathbf{sqrt}[\sum(\mathbf{z}_{\mathbf{lidari}} - \mathbf{z}_{\mathbf{RTKi}})^2/\mathbf{n}] \qquad \text{Eq. 2}$$

where, $z_{lidar\textit{i}}$ is the elevation of the lidar-derived DEM at *i*th RTK-GPS point, $z_{RTK\textit{i}}$ is the elevation of the *i*th RTK-GPS point, *n* is the number of RTK-GPS points, and *i* is an integer (1 - *n*). *RMSE* is a common statistic used to determine the difference between two datasets and can be interpreted as the standard deviation if errors are normally distributed (NDEP, 2004). If errors are not normally distributed, then interpretation of RMSE is simply the magnitude of error. FVA is the 95% confidence interval for RMS and is calculated by RMSE*1.96. PE is defined as the absolute value that is greater than 95% of dataset. RMSE and FVA are only appropriate if errors follow a normal distribution; otherwise PE should be used (Flood 2004). We calculated the skewness of error of the original and adjusted DEMs, and following Flood (2004), considered error distributions normal if skewness was within the range [-0.5, 0.5]. We also calculated mean error (ME) as a measure of bias in the original and adjusted lidar DEMs

$$\mathbf{ME} = \sum \frac{(\mathbf{lidar\ elevation} - \mathbf{RTKGPS\ elevation})}{\mathbf{n}} \qquad \text{Eq. 3}$$

where, n is the number of RTK-GPS points.

2.5. Model development

We used a site-specific, multivariate approach to model the relationship between lidar error, determined by subtracting the lidar DEM from the RTK-GPS data, NAIP-derived vegetation indices, and lidar elevation. Specifically, the model was defined as:

$$\mathbf{E = l + v + v^2 + l{*}v + l{*}v^2 + v^2{*}v + l{*}v{*}v^2} \qquad \text{Eq. 4}$$

where, *E* is the error (lidar elevation minus RTK-GPS elevation), *l* is the uncorrected lidar DEM elevation, and *v* is the NDVI. The model is fit to a training dataset using least-squares regression. We define this technique (Eq. 4) as the Lidar Elevation Adjustment with NDVI method (hereafter, the LEAN method).

To test the sensitivity of LEAN to particular RTK-GPS points, we ran a 100-fold cross validation analysis, randomly withholding 30% of the dataset for testing in each iteration. We calculated the average model correction from the individual cross-validation runs and reported the standard deviation of percent improvement in RMSE compared with the original lidar-derived DEM. To develop the best possible LEAN model, we trained the final NAIP model using the entire RTK-GPS dataset for each site.

We produced an adjusted DEM by applying LEAN to the lidar DEM and NDVI from the NAIP image. This was accomplished by converting the raster values of the aligned lidar DEM and NDVI datasets to numeric vectors and using the 'predict' function in base R to generate predictions of lidar error. The predicted lidar error was then subtracted from the original lidar DEM to produce an adjusted DEM of the marsh platform. To restrict model corrections to areas above the elevation of the mudflat and channels, we determined a site-specific marsh elevation height from inspection of the original lidar and NAIP imagery (Table 4). The final DEM was a mosaic of the LEAN-adjusted DEM above the marsh elevation height, and the original lidar DEM below the marsh elevation height. Our calibration RTK-GPS dataset did not include data from the channels (sides nor bottoms) or mudflats; we assumed any error in these areas were not due to dense vegetation and therefore LEAN was not appropriate for making adjustments to the DEM.

The timing of lidar acquisition is an important factor when considering effects of marsh vegetation on lidar returns. To assess the importance of concurrent (same year) lidar collection and NAIP imagery, we compared performance of models trained using NAIP images from different years than the lidar was flown at a subset of sites (Coon Island, Fagan, Mugu, Petaluma, Siletz, Tijuana). We analyzed the difference in RMSE between the correction models using a paired t-test (α=0.05).

Seasonal differences in vegetation height and density due to phenology are important in the context of vertical lidar error. To make our technique as broadly applicable as possible, we relied on readily available NAIP imagery that was collected in a different season than the lidar acquisition at several of our sites (Table 1). Our goal was not to directly infer aboveground biomass in our models, but rather to use the NAIP imagery as an indicator of spatial variability in vegetation height and density. Our approach assumes that the spatial variability detected in the NAIP imagery correlates with the variability in plant height and density when the lidar was flown (e.g., the location of dense vegetation in June is reasonably correlated with the location of dense vegetation in October). As we are relying on site-specific data to calibrate the correction model, only the relative magnitude of the NDVI signal across marsh is important, rather than the absolute value, thereby reducing the effect of seasonal differences in lidar and NAIP collection in our model. Caution should be used in areas with substantial senescence of vegetation when there is seasonal mismatch between lidar and multispectral imagery acquisitions.

2.6. Comparison of LEAN to Alternative Models

We compared LEAN to three published methods for adjusting lidar derived DEMs; minimum-bin gridding (MBG), mean error correction (MEC), and vegetation correction (VC). We compared LEAN to MBG and MEC across all our sites. For MBG, we acquired 5 m resolution lidar DEMs from NOAA's Coastal Data Viewer using the minimum grid averaging option. We then estimated the RMSE and mean error between the RTK-GPS elevation and elevation of the 5-m DEM at each RTK-GPS location. For MEC, we subtracted the mean difference between the 1-m lidar DEM and the RTK-GPS elevation from the original DEM. We then calculated the RMSE and ME for the MEC DEM. As MEC only uses RTK-GPS data, the difference in performance between MEC and LEAN represent the benefit for including NDVI from NAIP imagery into a correction model. For the three correction models (LEAN, MBG, MEC), we randomly subset the RTK data into 70% training and 30% testing datasets and used a 100-fold cross validation compare model performance. For two sites in SFB (China Camp and Coon Island), we also compared the RMSE of an existing VC DEM (Schile et al., 2014) with the RMSE from LEAN using our RTK data. The existing VC DEMs were created from the same SFB lidar dataset used in this study. We used paired t-tests (α=0.05) to compare the RMSE from the alternative methods with LEAN, and one-way ANOVAs to compare initial and adjusted RMSE across regions.

2.7. Power Analysis

Finally, we conducted a power analysis to estimate the minimum number of RTK-GPS points necessary to create a LEAN model that was statistically equivalent to the cross-validated LEAN model. For each site we randomly stratified RTK-GPS points into four classes, above and below mean lidar elevation and mean NDVI value, selecting an increasing number of points per class and replicating the subset 1000 times. We then determined the number of RTK-GPS points that would calibrate a model with a RMSE within 1 cm of the mean cross-validated RMSE. We calculated the mean, standard deviation and median of the lowest number of points per site. We conducted all analysis and model development using R version 3.2.2 (http://cran.r-project.org) and ArcGIS (version 10.1, ESRI, Redlands, CA).

3. Results

3.1 RTK-GPS Surveys

After removing points outside the marsh platform, a total of 17,740 RTK-GPS points across all sites were included in model development and analysis. Sites had an average of 96.0% (SD = 7.7) of their RTK-GPS elevations lower than the lidar DEM, indicating that vegetation biased lidar returns across all our study sites. Even when accounting for 5 cm of RTK-GPS measurement error, sites had an average of 88.9% (SD = 15.5) points that were lower than the lidar DEM. Across all sites, ME for lidar was 0.208 m (SD = 0.109) and RMSE was 0.231 m (SD = 0.010) (Table 3).

Table 3. Uncorrected lidar data root mean squared error (RMSE),initial mean error (ME), and fundamental vertical accuracy (FVA), 95th Percentile Error (PE, with standard deviation) from the training data, and mean (SD) Normalized Difference Vegetation Index (NDVI) for 17 study sites along the Pacific coast of the United States. Lidar error was calculated by subtracting RTK-GPS elevations from a 1-m lidar DEM for each study site. Sites where the skewness of the error distribution exceeds [-0.5, 0.5] are denoted with *.

Site	RMSE	ME	FVA	PE	NDVI Mean (SD)
Pacific Northwest					
Grays Harbor	0.466	0.419	0.912	0.871 (0.017)	0.228 (0.156)
Willapa*	0.392	0.382	0.768	0.501 (0.008)	0.203 (0.101)
Siletz*	0.304	0.269	0.596	0.434 (0.010)	0.410 (0.067)
Bull Island*	0.145	0.078	0.284	0.476 (0.15)	0.138 (0.099)
Bandon*	0.118	0.016	0.232	0.243 (0.004)	0.289 (0.127)
PNW Mean	0.285	0.233	0.560	0.505 (0.011)	0.254 (0.057)
San Francisco Bay					
Petaluma*	0.289	0.282	0.566	0.382 (0.004)	0.259 (0.058)
Black John	0.278	0.264	0.546	0.418 (0.011)	0.222 (0.053)
San Pablo	0.265	0.253	0.520	0.374 (0.003)	0.385 (0.094)
Fagan	0.256	0.242	0.502	0.376 (0.006)	0.339 (0.094)
Coon Island	0.273	0.260	0.535	0.401 (0.007)	0.348 (0.075)
China Camp	0.233	0.228	0.457	0.309 (0.003)	0.155 (0.047)
Corte Madera	0.182	0.228	0.357	0.367 (0.008)	0.218 (0.068)
SFB Mean	0.254	0.251	0.498	0.375 (0.006)	0.275 (0.070)
Southern California					
Morro*	0.109	0.082	0.214	0.216 (0.002)	0.011 (0.137)
Mugu	0.155	0.154	0.303	0.266 (0.003)	0.238 (0.142)

Seal Beach*	0.168	0.147	0.329	0.295 (0.003)	0.347 (0.123)
Newport	0.183	0.140	0.358	0.352 (0.008)	0.235 (0.126)
Tijuana*	0.113	0.084	0.221	0.209 (0.006)	0.239 (0.074)
SCA Mean	0.145	0.121	0.285	0.268 (0.004)	0.214 (0.120)
Overall Mean	0.231	0.208	0.453	0.382 (0.007)	0.251 (0.097)

3.2 Lidar data

Lidar error varied across study regions and between sites within regions (Fig. 2). Grays Harbor and Willapa had higher initial lidar RMSE, while Bull Island, Bandon, Mugu and Tijuana had lower initial RMSE. The higher point density of the PNW lidar dataset (8 pts/m vs. 1 pt/m) did not appear to have an effect on lidar error, as Willapa and Grays Harbor had the highest lidar error while Bull Island and Bandon had some of the lowest error.

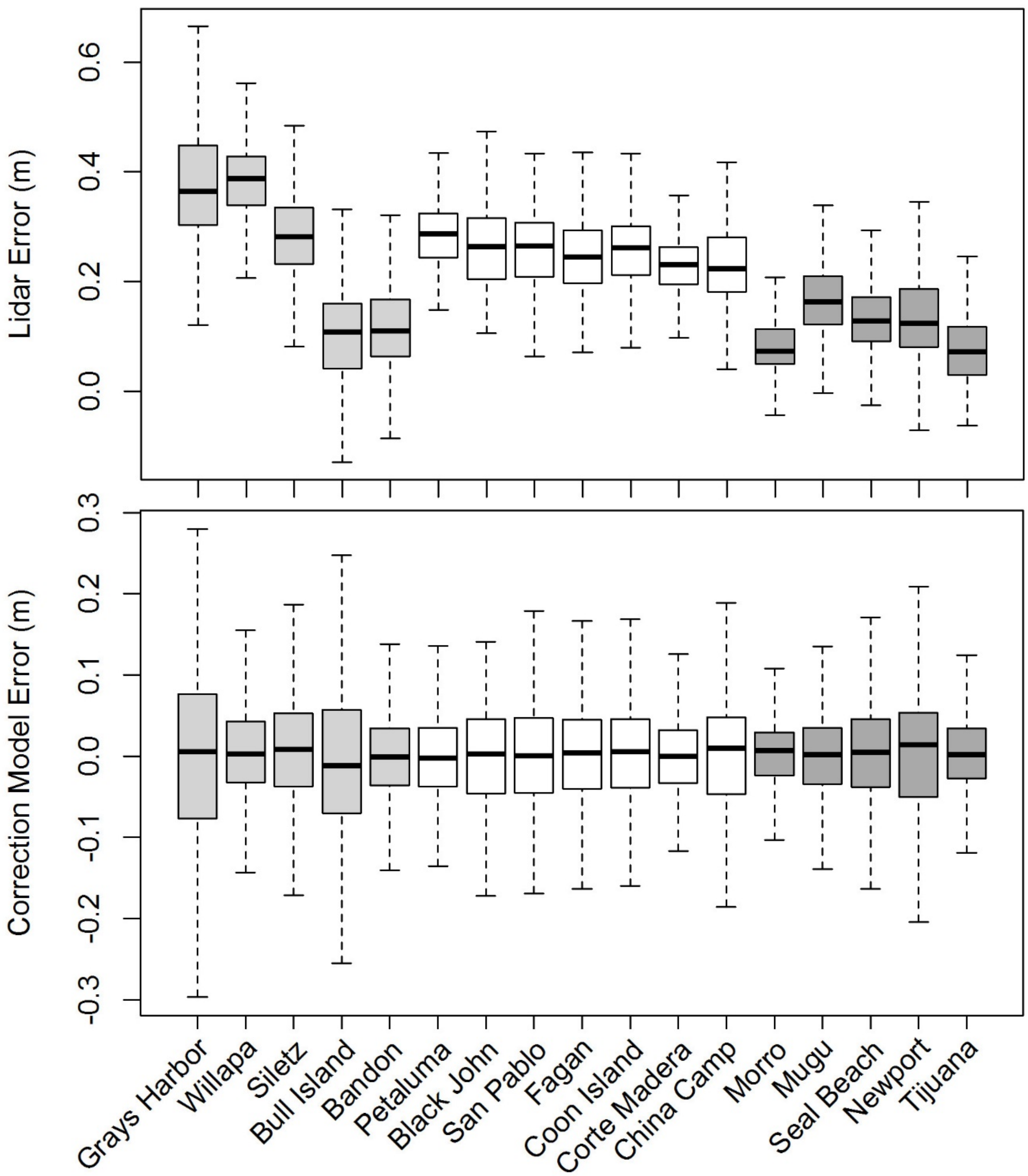

Fig. 2. Boxplot of uncorrected lidar error (top) and errors from Lidar Elevation Adjustment using NDVI (LEAN) corrections (bottom) across study sites. Lidar error was calculated by subtracting RTK-GPS elevation from the lidar DEM. Box shading designates region (light grey: Pacific Northwest, white: San Francisco Bay, dark grey: Southern California). Sites are ordered from north to south.

Initial RMSE across the PNW sites and the SFB sites were significantly greater than the initial RMSE across the SCA sites (PNW vs. SCA, $t = 2.39$, $df = 8$, $p = 0.044$; SFB vs. SCA, $t =$

5.29, df = 10, $p < 0.0001$). While the PNW sites had a larger range of initial RMSE, it was not significantly different than the SFB initial RMSE ($t = 0.78$, df = 10, $p = 0.45$). Mean initial RMSE across all site was 0.231 m (sd = 0.098).

3.3. DEM correction

The LEAN model reduced lidar bias by an average of 58.5% across all sites, ranging from 40-75% (Table 3). The mean RMSE after LEAN correction across all sites was 0.072 m (sd = 0.018). LEAN successfully eliminated the positive bias in lidar error (Fig. 3); ME across all sites was 0 (sd = 0.065). Mean percent improvement in RMSE using LEAN varied significantly across regions (ANOVA, $F_{2, 14} = 5.05$, $p = 0.022$).

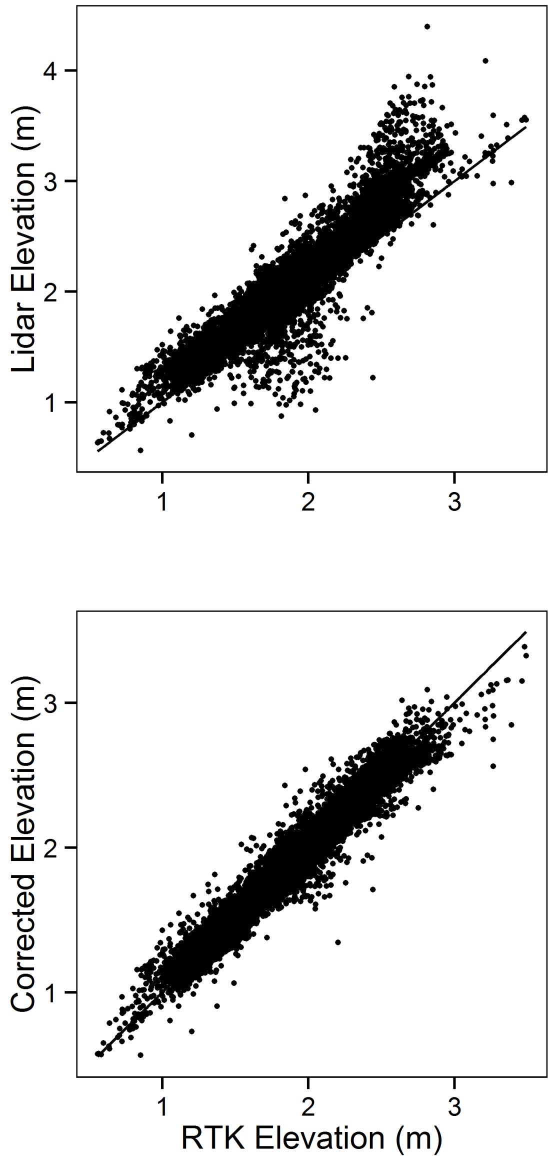

Fig. 3. Positive bias in lidar DEM before Lidar Elevation Adjustment using NDVI (LEAN) correction (top) and after LEAN correction (bottom), with a 1:1 line. Units in m, NAVD88.

Table 4. Lidar Elevation Adjustment using NDVI (LEAN) corrected DEM accuracy statistics for 17 tidal marshes along the Pacific Coast of the United States. Root mean squared error (RMSE) for LEAN-corrected DEMs using all RTK-GPS points, Mean RMSE (standard deviation) from 100-fold cross validation, mean error (ME), fundamental vertical accuracy (FVA), 95th Percentile Error (PE, with SD), and percent improvement in PE. Sites where the skewness of the error distribution exceeds [-0.5, 0.5] are denoted with *.

Site	RMSE (All Pnts)	RMSE Mean (SD)	ME	FVA	PE Mean (SD)	% Imp. PE	Mudflat Elevation (m)
Pacific Northwest							
Grays Harbor	0.118	0.121 (0.005)	1.77E-15	0.236	0.231 (0.010)	73.4	2.1
Willapa	0.079	0.072 (0.011)	5.50E-16	0.141	0.126 (0.015)	74.9	2.2
Siletz*	0.090	0.092 (0.006)	-5.86 E-15	0.181	0.182 (0.019)	58.0	2.3
Bull Island*	0.076	0.080 (0.006)	-2.01E-16	0.156	0.150 (0.009)	42.5	1.7
Bandon	0.069	0.071 (0.004)	8.93E-16	0.138	0.139 (0.007)	42.6	1.5
PNW Mean	0.086	0.087 (0.006)	0.000	0.170	0.166 (0.013)	58.3	-
San Francisco Bay							
Petaluma*	0.056	0.069 (0.028)	2.00E-15	0.135	0.110 (0.009)	71.2	1.3
Black John	0.071	0.081 (0.012)	3.01E-15	0.158	0.136 (0.014)	67.4	1.3
San Pablo	0.070	0.075 (0.011)	1.04E-14	0.146	0.142 (0.014)	62.1	1.3
Fagan	0.064	0.070 (0.013)	3.36E-15	0.138	0.127 (0.013)	66.3	1.3
Coon Island*	0.070	0.071 (0.004)	-9.86E-15	0.140	0.144 (0.011)	64.0	1.3
China Camp	0.051	0.054 (0.004)	7.74E-16	0.106	0.099 (0.008)	67.9	1.3
Corte Madera	0.057	0.062 (0.009)	-1.77E-15	0.122	0.150 (0.012)	59.0	1.3
SFB Mean	0.063	0.069 (0.012)	0.000	0.135	0.130 (0.012)	65.4	-
Southern California							
Morro	0.056	0.057 (0.003)	1.06E-15	0.112	0.113 (0.008)	47.8	1.3
Mugu	0.049	0.049 (0.001)	-5.94E-16	0.096	0.107 (0.005)	59.7	1.3
Seal Beach	0.074	0.074 (0.002)	7.39E-15	0.146	0.149 (0.006)	49.6	1.3
Newport*	0.102	0.104 (0.008)	-5.61E-16	0.203	0.211 (0.019)	40.0	1.2
Tijuana*	0.064	0.065 (0.004)	-1.94E-15	0.127	0.123 (0.011)	41.1	1.3
SCA Mean	0.069	0.070 (0.004)	0.000	0.137	0.142 (0.010)	47.6	-
Overall Mean	0.072	0.076 (0.008)	0.000	0.138	0.143 (0.011)	58.1	-

3.4. Alternative Models

Mean RMSE across the sites calibrated with alternative year NDVI data was 0.059 m (SD=0.005), while the mean RMSE of models calibrated with the NDVI from the same year as the lidar was 0.065 m (SD=0.009). Correlation in NDVI between years ranged from moderate

(0.52) to low (0.028) with a mean of 0.20. There was no significant difference in RMSE between the alternative NDVI year models and the models with the original NDVI (paired t-test; $t = 1.50$, $df = 4$, $p = 0.103$).

The MGB, MEC, and VC lidar correction methods reduced the RMSE of the lidar data, but not as much as the LEAN method when compared to the RTK-GPS elevation points. Correcting the lidar DEM with the MEC reduced RMSE to an average of 0.096 m (CI = 0.188 m), that was significantly greater than the RMSE using LEAN (paired t-test, $t = 2.79$, $df = 16$, $p = 0.007$; Table 4). MBG at 5 m resolution increased mean RMSE across sites to 0.271 m, and ME was positively biased at 0.065 m. At a few sites (Newport, Tijuana), MBG reduced signed mean error to within ±5 cm of 0, however, the RMSE was > 0.2 m (Table 5). At China Camp, RMSE of the VC DEM was 0.12 m, compared to 0.051 m RMSE achieved using LEAN, while at Coon Island, RMSE of the VC DEM was 0.084 m compared to a RMSE of 0.070 m using LEAN.

Table 5. Estimated error for alternative methods for correcting lidar digital terrain models. Mean Error Correction (MEC) root mean error squared (RMSE, m; with standard deviation), 5 m minimum bin gridding (MBG) RMSE (m; SD), and 5 m MBG mean error (m; SD) are reported from the 100-fold cross validation models.

Site	MEC RMSE	MBG RMSE	MBG Mean Error
Pacific Northwest			
Grays Harbor	0.204 (0.010)	0.360 (0.014)	0.271 (0.012)
Willapa	0.089 (0.010)	0.312 (0.020)	0.227 (0.014)
Siletz	0.101 (0.006)	0.226 (0.012)	0.089 (0.008)
Bull Island	0.092 (0.007)	0.259 (0.020)	-0.062 (0.011)
Bandon	0.141 (0.008)	0.258 (0.019)	-0.075 (0.011)
PNW mean	*0.125 (0.008)*	*0.283 (0.016)*	*0.090 (0.011)*
San Francisco Bay			
Petaluma	0.064 (0.004)	0.286 (0.020)	0.162 (0.015)
Black John	0.089 (0.006)	0.245 (0.026)	0.153 (0.022)
San Pablo	0.080 (0.005)	0.259 (0.025)	0.113 (0.019)
Fagan	0.083 (0.004)	0.224 (0.016)	0.077 (0.014)
Coon Island	0.084 (0.004)	0.288 (0.021)	0.105 (0.016)
China Camp	0.054 (0.003)	0.251 (0.022)	0.106 (0.014)
Corte Madera	0.063 (0.007)	0.278 (0.013)	0.114 (0.014)
SFB mean	*0.074 (0.005)*	*0.262 (0.021)*	*0.119 (0.016)*
Southern California			
Morro	0.072 (0.004)	0.213 (0.012)	-0.051 (0.006)
Mugu	0.064 (0.002)	0.209 (0.006)	0.135 (0.006)
Seal Beach	0.081 (0.002)	0.315 (0.011)	-0.083 (0.008)
Newport	0.118 (0.010)	0.240 (0.022)	0.000 (0.011)
Tijuana	0.075 (0.002)	0.229 (0.021)	-0.033 (0.013)
SCA mean	*0.082 (0.005)*	*0.241 (0.015)*	*-0.007 (0.009)*

3.5. Power Analysis

Across sites, an average of 118.3 (SD = 56.7) total RTK-GPS ground points, stratified by mean elevation and NDVI, resulted in a LEAN model RMSE that was within 1 cm of the mean cross-validated RMSE, while an average of 87 total RTK-GPS points resulted in models within 2 cm of the mean RMSE. Three sites (Corte Madera, China Camp, and Willapa) did not converge on the mean cross-validated RMSE and were excluded from the average. Grays Harbor needed the highest number of RTK-GPS points (236), while Black John required only 52 to build a robust LEAN model. The median number of RTK-GPS points needed was 104. Figures for each site are provided as supplemental information (Fig. S1-S3).

4. Discussion

Consistent with previous studies, we found that lidar overestimated tidal marsh surface elevation at all our study sites. The bias ranged from 0.11-0.47 m (RMSE), which at the high end exceeds values for sites in South Carolina (0.15 m; Schmid et al., 2011) and Georgia (0.23 m; Hladik and Alber 2012), but is less than the bias found in a Florida marsh along the Gulf of Mexico (0.65 m, Medeiros et al., 2015). Lidar bias in our study varied by study region, likely because each region has distinct dominant vegetation communities (Table 1) with different canopy heights and densities (Schmid et al., 2011; Hladik and Alber, 2012; McClure et al., 2016). Additionally, lidar was acquired in different seasons which may also explain regional differences in initial error.

The LEAN model reduced positive bias in lidar DEMs 40-75% across the 17 tidal marshes, with low variation in final RMSE (Fig. 4). By relying on a statistical approach to lidar error correction, LEAN was insensitive to temporal mismatches between NDVI and lidar datasets, evidenced by the low standard deviation in final RMSE across sites (0.018 m; an 82% reduction in RMSE variation across sites). LEAN successfully reduced lidar error across a wide variety of dominant marsh vegetation communities while maintaining high spatial resolution, and the mean RMSE of 0.072 m across all our sites is lower than previous attempts to correct lidar in tidal marshes. In comparisons with other correction methods, the accuracy of our LEAN model was followed by MEC (0.096 m RMSE), VC (0.10 m RMSE, for China Camp and Coon Island), and MBG (0.271 m RMSE). Unexpectedly, MBG resulted in increased mean RMSE across sites, likely due to the addition of channel and mudflat features within the 5 m pixels. Because we modeled total lidar elevation errors, LEAN accounts for both random sensor error and the systematic influence of dense vegetation canopies. Our focus was to correct the positive bias across the marsh platform as our RTK-GPS dataset did not include points within channels or on mudflats; additional work is warranted to address lidar error in these important marsh features.

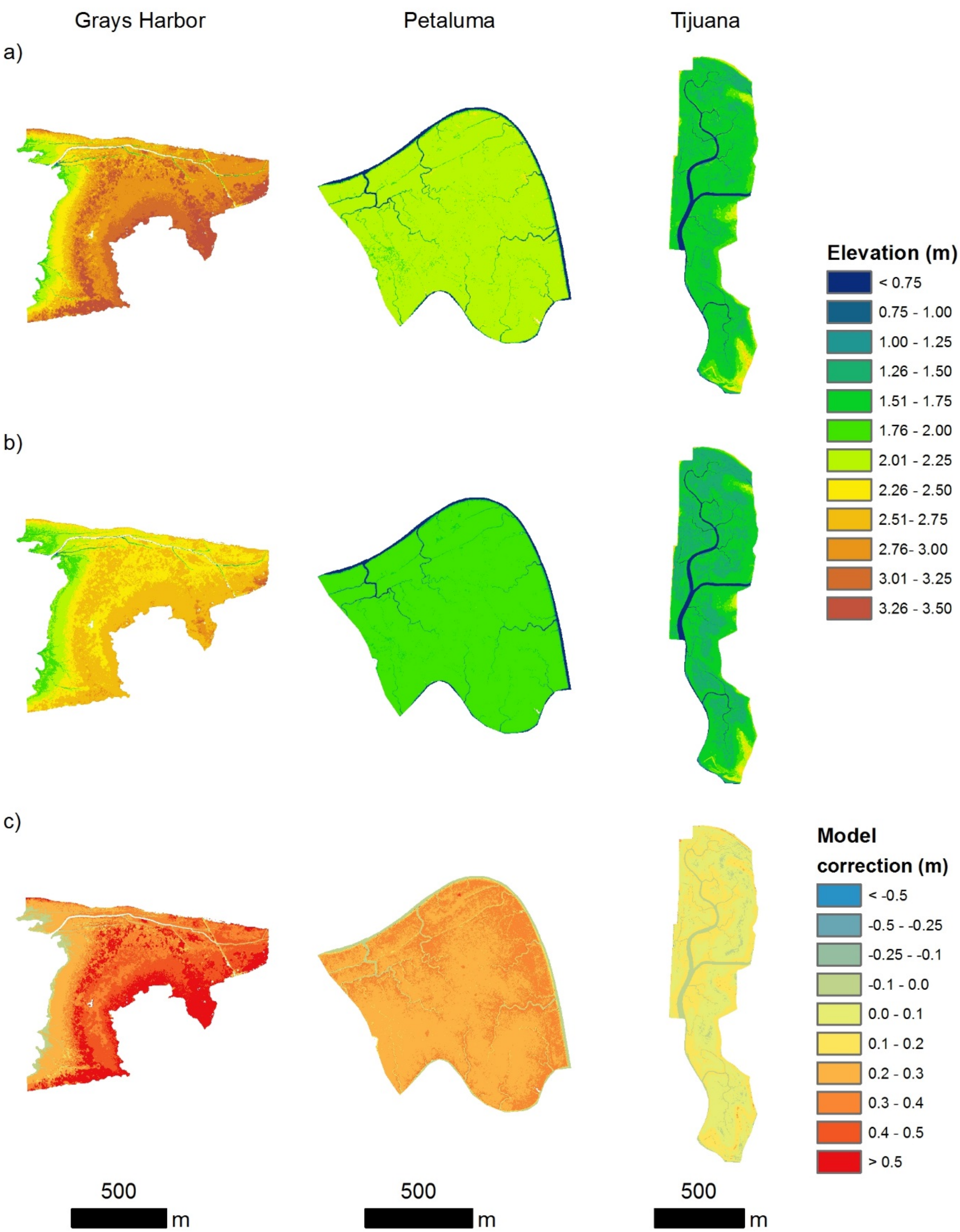

Fig. 4. Example results from each region (Pacific Northwest: Grays Harbor; San Francisco Bay: Petaluma; Southern California: Tijuana. (a) Uncorrected lidar digital terrain model (DEM; (b) model adjusted DEM, and (c) total adjustment. Elevation in m, National Vertical Datum of 1988.

LEAN (RMSE of 0.051 m) outperformed two prior efforts to correct lidar at China Camp that used vegetation correction methods. Schile et al. (2014) used the mean error for the dominant species (*Salicornia pacifica*) to correct the lidar DEM and achieved a RMSE of 0.12 m. McClure et al. (2016) used a more detailed vegetation map and correction factors for five species of plants to create a modified DEM with a RMSE of 0.098 m. LEAN likely outperforms VC methods because NDVI captures variation in both plant canopy height and aboveground biomass that can influence lidar reflectance and canopy penetration. More important than the relatively small improvements in accuracy is that LEAN does not require time-consuming vegetation surveys and airborne photo interpretation or expensive hyperspectral data to develop correction factors for individual species or communities, making LEAN relatively easy and inexpensive to implement.

The temporal mismatch between the RTK-GPS surveys and lidar acquisition is a potential source of uncertainty. Annual changes in tidal marsh elevations, however, occur at the millimeter-scale (2-8 mm/yr at our study sites, Thorne et al., 2015, Thorne et al., 2016) and the amount of instrument error in both the RTK-GPS (~2 cm) and lidar (>4 cm) is too large to robustly detect marsh elevation changes over relatively short time periods. A greater temporal mismatch is not necessarily an issue, provided the RTK-GPS surveys occur after the lidar acquisition; adjustments to the original lidar DEM using LEAN can be interpreted as both correcting for dense vegetation and updating the DEM for changes in surface elevation.

Lidar-derived DEMs corrected using LEAN can be confidently used in mid-term (2050) SLR projections. NOAA recommends that DEMs used in sea-level rise (SLR) projections should be at least twice as accurate (using the 95$^{\%}$ confidence interval, RMSE*1.96) as the SLR increment being modeled (NOAA, 2010). Mean SLR projections for our study regions and the recommended DEM accuracies for 2030, 2050 and 2100 are provided (Table 6). The uncorrected lidar appears to have sufficient accuracy for 100-year projections across our SCA sites, but not our SFB or PNW sites illustrating that uncorrected lidar should be used with caution for assessing flooding risk to tidal marshes and other coastal zones without a correction for vegetation. Technological and analysis advances are necessary before lidar is capable of the accuracy needed for short-term (2030) projections, especially for areas with relatively low SLR projections as in the PNW.

Table 6. Sea-level rise (SLR) projections (NRC, 2012) and recommended digital elevation model accuracy (root mean squared error [RMSE]) for San Francisco Bay (SFB), Southern California (SCA), and Pacific Northwest (PNW) study sites.

	SLR Projection (cm)		RMSE (cm)	
Year	SFB/SCA	PNW	SFB/SCA	PNW
2030	14.4	6.8	3.8	1.7
2050	28.0	17.2	7.1	4.3
2100	91.9	63.3	23.2	16.0

Reliance on unadjusted lidar has consequences for both short and long term ecological applications for low slope tidal marshes. In the short term, LEAN-adjusted DEMs can correct projections of inundation frequency during the 24-hour tide cycle. For example, at three representative sites the estimate of inundation duration for the mean elevation of each site ranged from 1.3 to 4 times longer using the LEAN adjusted DEM versus uncorrected lidar (results not shown). Small changes in duration of inundation may change productivity (Janousek et al., 2016) and community composition of marsh plants (Kirwan and Guntenspergen, 2012; Langley et al., 2013), and affect wildlife that rely on intertidal habitats for nesting, foraging, and refugia (Shaughnessy et al., 2012; Takekawa et al., 2012).

In the long term, unadjusted DEMs can bias predictions of marsh persistence under SLR. Models like the Sea Level Affecting Marshes Model (SLAMM, Craft et al., 2009), Marsh Equilibrium Model (MEM; Morris et al., 2002), and Wetland Accretion Model for Ecosystem Resilience (WARMER, Swanson et al., 2013) all require an initial DEM with accurate starting elevation upon which to make future elevation projections under SLR. Sensitivity analysis of WARMER results indicate that 30-50% of the variance in final elevation is due to initial elevation (Thorne et al., 2015, Thorne et al., 2016). In comparing WARMER results to 2110 with uncorrected DEMS and LEAN adjusted DEMs for three of our study sites (Grays Harbor, Petaluma, and Tijuana), we found WARMER predicted a loss of high marsh habitat 30 years earlier at Grays Harbor with the LEAN adjustment. At Petaluma, high marsh classified with the lidar DEM was reclassified as mid marsh with the LEAN DEM, and the transition to mudflat was predicted to be 10 years earlier, and at Tijuana the amount of habitat currently classified as high marsh was reduced by 46%, illustrating the importance of correcting lidar for marsh vegetation (results not shown, marsh classifications from Thorne et al. 2015 and Thorne et al., 2016).

LEAN was also robust to variation in NAIP image availability. We found that LEAN calibrated with NAIP imagery from years other than those of the lidar data performed as well as the LEAN corrections using lidar data and NAIP imagery from the same year. Due to the variance in correlation of NDVI between images, however, a LEAN model should not be calibrated with a NAIP image from one year and projected using a different year. Theoretically, the shorter the timespan between lidar and NAIP (or NDVI) data acquisitions, the more accurate the model corrections; however, the results seem robust to differences of several years, likely due site-specific model calibration and low interannual variation of marsh perennials. In addition, NAIP images may be acquired during high tides or cloudy conditions in some years which will affect NDVI values, thus the capability of LEAN to use images from any recent year is especially useful.

We suggest taking at least 40 RTK-GPS points per vegetation class (± mean elevation and ± mean NVDI) to produce a robust DEM using LEAN, and up to 60 per class if the marsh has greater spatial variation in plant density and height. This number of sample points (~120) would also be sufficient to run a cross-validation for assessing model performance. In addition, separate model calibrations should be performed in areas that have very different dominant vegetation. For instance, we recommend modeling salt, brackish, and freshwater marshes within an estuary separately as the relationship between lidar error and NDVI may vary across these different marsh types. From the power analysis, we found no relationship between marsh area and number of RTK-GPS needed for LEAN calibration. While our sites were generally small in area, this result highlights the importance of capturing the variation in NDVI and initial lidar DEM with the RTK-GPS surveys rather than ensuring a specific density of points. Additional RTK-GPS points should be collected in areas with complex vegetation communities and high variability in NDVI. Finally, to avoid errors related to lidar DEM resolution, we advise surveying elevation at least 1 pixel (m) away from areas with steep slope such as channels and scarps.

5. Conclusion

Airborne lidar provides invaluable elevation data by generating thousands of data points per hectare. However, some correction to lidar DEMs is required to offset the positive bias caused by the dense vegetation canopy in tidal marshes. The LEAN method for correcting lidar data requires a relatively small dataset of ground elevation points for calibration and a spatial map indicative of vegetation density (e.g., NDVI). The power analysis showed that on average 120 RTK-GPS points were necessary for a robust LEAN model.

LEAN could be applied to other habitat types where dense vegetation obstructs the ground surface and high vertical accuracy is needed. So long as a sufficient number of RTK-GPS data are available, our statistical approach to lidar correction should be robust. The flat terrain and dynamic coastal landscape necessitates that tidal marsh DEMs be highly accurate to be useful across ecological, geomorphological, and engineering applications. NDVI derived from commercially available satellite images could be used in place of the NAIP airborne images to expand our method to areas in the world not covered by NAIP imagery.

Acknowledgments

The authors would like to thank all the technicians who helped collect the RTK-GPS data for this study, including C. Freeman, K. Powelson, K. Lovett, L. Curry, P. Elson, T. Henner, and T. Bui. Thanks also to A. Nolin, C. Janousek and J. Vogeler for valuable conversations, comments, and insight. E. Harrington and C. Malachowski provided editorial assistance on earlier drafts of the manuscript. Special thanks to L. Schile for providing the vegetation corrected DEMs of China Camp and Coon Island for comparisons to LEAN. We would also like to thank DOI U.S. Geological Survey, Western Ecological Research Center, National Climate Change and Wildlife Science Center, the National Oceanic and Atmospheric Administration EESLR program (grant ID NA15NOS4780171), Northwest Climate Science Center (NWCSC), Southwest Climate Science Center, U.S. Fish & Wildlife Service North Pacific and California Landscape Conservation Cooperatives, Oregon State University and the NWCSC fellowship for funding support. Any use of trade, product, or firm names in this publication is for descriptive purposes only and does not imply endorsement by the U.S. government.

Literature Cited

Adam, E., Mutanga, O., and Rugege, D. (2010). Multispectral and hyperspectral remote sensing for identification and mapping of wetland vegetation: A review. *Wetl. Ecol. Manag.* 18, 281–296. doi:10.1007/s11273-009-9169-z.

Butzeck, C., Eschenbach, A., Gröngröft, A., Hansen, K., Nolte, S., and Jensen, K. (2014). Sediment Deposition and Accretion Rates in Tidal Marshes Are Highly Variable Along Estuarine Salinity and Flooding Gradients. *Estuaries and Coasts*, 434–450. doi:10.1007/s12237-014-9848-8.

Cahoon, D. R., and Reed, D. J. (1995). Relationships amoung marsh surface topography, hydroperoid, and soil accretion in a deteriorating Louisana salt marsh. *J. Coast. Res.* 11, 357–369.

Chavez, P. S. J. (1988). An improved dark-object subtraction technique for amtopshiec scattering correction of multispectral data. *Remote Sens. Environ.* 24, 459–479.

Craft, C., Clough, J., Ehman, J., Jove, S., Park, R., Pennings, S., Guo, H., and Machmuller, M. (2009). Forecasting the effects of accelerated sea-level rise on tidal marsh ecosystem services. *Front. Ecol. Environ.* 7, 73–78. doi:10.1890/070219.

Federal Geographic Committee. (1998). Geospatial positioning accuracy standards part 3: National standard for spatial data accuracy. FGDC-STD-007 3-1998, http://www.fgdc.gov/standards/projects/FGDC-standards-projects/accuracy/part3/chapter3.

Filella, I., Peñuelas, J., Llorens, L., and Estiarte, M. (2004). Reflectance assessment of seasonal and annual changes in biomass and CO2 uptake of a Mediterranean shrubland submitted to experimental warming and drought. *Remote Sens. Environ.* 90, 308–318. doi:10.1016/j.rse.2004.01.010.

Flood, M (ed.). (2004). Vertical accuracy reporting for lidar data, version 1.0. ASPRS Lidar Committee (PAD), 20p. http://asprs.org/a/society/committee/lidar/Downloads/Vertical_Accuracy_Reporting_for_Lidar_Data.pdf

Foxgrover, B. A. C., Finlayson, D. P., and Jaffe, B. E. (2011). 2010 Bathymetry and Digital Elevation Model of Coyote Creek and Alviso Slough, South San Francisco Bay, California. *U.S. Geol. Surv. Open File Rep.*, 20.

Gamon, J. A., Field, C. B., Goulden, M. L., Griffin, K. L., Hartley, A., Joel, G., Penuelas, J., and Valentini, R. (1995). Relationships Between NDVI , Canopy Structure , and Photosynthesis in Three Californian Vegetation Types. *Ecol. Appl.* 5, 28–41.

Hackney, C. T., Brady, S., Stemmy, L., Boris, M., Dennis, C., Hancock, T., O'Bryon, M., Tilton, C., and Barbee, E. (1996). Does intertidal vegetation indicate specific soil and hydrologic conditions. *Wetlands* 16, 89–94. doi:10.1007/BF03160649.

Hladik, C., and Alber, M. (2012). Accuracy assessment and correction of a LIDAR-derived salt marsh digital elevation model. *Remote Sens. Environ.* 121, 224–235. doi:10.1016/j.rse.2012.01.018.

Hladik, C., Schalles, J., and Alber, M. (2013). Salt marsh elevation and habitat mapping using hyperspectral and LIDAR data. *Remote Sens. Environ.* 139, 318–330. doi:10.1016/j.rse.2013.08.003

Hodgson, M. E., and Bresnahan, P. (2004). Accuracy of Airborne Lidar-Derived Elevation : Empirical Assessment and Error Budget. *Photogramm. Eng. Remote Sensing* 70, 331–339.

Janousek, C. N., Buffington, K. J., Thorne, K. M., Gutenspergen, G. R., Takekawa, J. Y., Dugger B. D. (2016). Potential effects of sea-level rise on plant productivity:species-specific responses in northeast Pacific tidal marshes. *Marine Ecology Progress Series*, 548: 111-125.

Kane, V. R., McGaughey, R. J., Bakker, J. D., Gersonde, R. F., Lutz, J. a., and Franklin, J. F. (2010). Comparisons between field- and LiDAR-based measures of stand structural complexity. *Can. J. For. Res.* 40, 761–773. doi:10.1139/X10-024.

Kirwan, M. L., and Guntenspergen, G. R. (2012). Feedbacks between inundation, root production, and shoot growth in a rapidly submerging brackish marsh. *J. Ecol.* 100, 764–770. doi:10.1111/j.1365-2745.2012.01957.x.

Kirwan, M., and Temmerman, S. (2009). Coastal marsh response to historical and future sea-level acceleration. *Quat. Sci. Rev.* 28, 1801–1808. doi:10.1016/j.quascirev.2009.02.022.

Kolker, A. S., Goodbred, S. L., Hameed, S., and Cochran, J. K. (2009). High-resolution records of the response of coastal wetland systems to long-term and short-term sea-level variability. *Estuar. Coast. Shelf Sci.* 84, 493–508. doi:10.1016/j.ecss.2009.06.030.

Langley, A. J., Mozdzer, T. J., Shepard, K. A., Hagerty, S. B., and Patrick Megonigal, J. (2013). Tidal marsh plant responses to elevated CO2, nitrogen fertilization, and sea level rise. *Glob. Chang. Biol.* 19, 1495–1503. doi:10.1111/gcb.12147.

Maune, D. F., Maitra, J. B., and McKay, E. J. (2007). Accuracy standards & guidelines. In: Maune D. (ed.), Digital Elevation Model Technologies and Applications. The DEM Users Manual, 2nd Edition. Bethesda, Maryland: American Society for Photogrammetry and Remote Sensing, pp. 65-97.

McClure, A. Liu, X., Hines, E., and Ferner, M. C. (2016). Evaluation of error reduction techniques on a LIDAR-derived salt marsh digital elevation model. *J. Coast Res.* 32:2, 424-433.

Medeiros, S., Hagen, S., Weishampel, J., and Angelo, J. (2015). Adjusting Lidar-Derived Digital Terrain Models in Coastal Marshes Based on Estimated Aboveground Biomass Density. *Remote Sens.* 7, 3507–3525. doi:10.3390/rs70403507.

Mitasova, H., Overton, M. F., Recalde, J. J., Bernstein, D. J., and Freeman, C. W. (2009). Raster-Based Analysis of Coastal Terrain Dynamics from Multitemporal Lidar Data. *J. Coast. Res.* 252, 507–514. doi:10.2112/07-0976.1.

Montané, J. M., and Torres, R. (2006). Accuracy Assessment of Lidar Saltmarsh Topographic Data Using RTK GPS. *Photogramm. Eng. Remote Sens.*, 961–967.

Morris, J. T., Sundareshwar, P. V., Nietch, C., Kjerfve, B., and Cahoon, D. R. (2002). Responses of coastal wetlands to rising sea level ¨. *Ecology* 83, 2869–2877.

Myneni, R. B., Hall, F. G., Sellers, P. J., and Marshak, A. L. (1995). Interpretation of spectral vegetation indexes. *IEEE Trans. Geosci. Remote Sens.* 33, 481–486. doi:10.1109/36.377948.

National Digital Elevation Program (NDEP). (2004). Guidelines for Digital Elevation Data, Version 1.0. 10 May 2004, 93 p. http://www.ndep.gov/NDEP_Elevation_Guidelines_Ver1_10_May2004.pdf

National Oceanic and Atmospheric Administration (NOAA). (2010). Technical considerations or the use of geospatial data in sea level change mapping and assessment. Silver Spring, Maryland: U.S. Department of Commerce, NOAA NOA Technical Report, NOAA National Ocean Service, 141 p. http://www.csc.noaa.gov/digitalcoast/_/pdf/SLC_Technicial_Considerations_Document.pd p.

Parrish, C. E., Rogers, J. N., and Calder, B. R., (2014). Assessment of waveform features for lidar uncertainty modeling in a coastal salt marsh environment. *IEEE Geoscience and Remote Sensing Letters*, 11:2, 569-573.

Pennings, S. C., Callaway, R. M., Apr, N., and Way, M. C. (1992). Salt Marsh Plant Zonation: The Relative Importance of Competition and Physical Factors. *Ecology* 73, 681–690.

Pettorelli, N., Vik, J. O., Mysterud, A., Gaillard, J. M., Tucker, C. J., and Stenseth, N. C. (2005). Using the satellite-derived NDVI to assess ecological responses to environmental change. *Trends Ecol. Evol.* 20, 503–510. doi:10.1016/j.tree.2005.05.011.

Rosso, P. H., Ustin, S. L., and Hastings, A. (2005). Mapping marshland vegetation of San Francisco Bay, California, using hyperspectral data. *Int. J. Remote Sens.* 26, 5169–5191. doi:10.1080/01431160500218770.

Sadro, S., Gastil-Buhl, M., and Melack, J. (2007). Characterizing patterns of plant distribution in a southern California salt marsh using remotely sensed topographic and hyperspectral data and local tidal fluctuations. *Remote Sens. Environ.* 110, 226–239. doi:10.1016/j.rse.2007.02.024.

Schile, L. M., Callaway, J. C., Morris, J. T., Stralberg, D., Thomas Parker, V., and Kelly, M. (2014). Modeling tidal marsh distribution with sea-level rise: Evaluating the role of vegetation, sediment, and upland habitat in marsh resiliency. *PLoS One* 9. doi:10.1371/journal.pone.0088760.

Schmid, K. A., Hadley, B. C., and Wijekoon, N. (2011). Vertical Accuracy and Use of Topographic LIDAR Data in Coastal Marshes. *J. Coast. Res.* 275, 116–132. doi:10.2112/JCOASTRES-D-10-00188.1.

Shaughnessy, F. J., Gilkerson, W., Black, J. M., Ward, D. H., and Petrie, M. (2012). Predicted eelgrass response to sea level rise and its availability to foraging Black Brant in Pacific coast estuaries. *Ecol. Appl.* 22, 1743–1761. doi:10.1890/11-1083.1.

Silvestri, S., Defina, A., and Marani, M. (2005). Tidal regime, salinity and salt marsh plant zonation. *Estuar. Coast. Shelf Sci.* 62, 119–130. doi:10.1016/j.ecss.2004.08.010.

Swanson, K. M., Drexler, J. Z., Schoellhamer, D. H., Thorne, K. M., Casazza, M. L., Overton, C. T., Callaway, J. C., and Takekawa, J. Y. (2013). Wetland Accretion Rate Model of Ecosystem Resilience (WARMER) and Its Application to Habitat Sustainability for Endangered Species in the San Francisco Estuary. *Estuaries and Coasts* 37, 476–492. doi:10.1007/s12237-013-9694-0.

Takekawa, J. Y, Thorne, K. M., Buffington, K. J., Spragens, K. A., Swanson, K. M., Drexler, J. Z., Schoellhamer, D. H., Overton, C. T., and Casazza, M. L. (2013). Final report for sea-level rise response modeling for San Francisco Bay estuary tidal marshes. U. S. Geological Survey Open File Report 2013-1081, 161 p.

Takekawa, J. Y., Woo, I., Thorne, K. M., Buffington, K. J., Nur, N., Casazza, M. L., and Ackerman, J. T. (2012). “Chapter 12: Bird communities: effects of fragmentation, disturbance, and sea level rise on population viability,” in *Ecology, Conservation, and*

Restoration of Tidal Marshes: The San Francisco Estuary, 175–194. doi:http://dx.doi.org/10.1525/california/9780520274297.003.0012

Thorne, K. M., Dugger, B. D., Buffington, K. J., Freeman, C. M., Janousek, C. N., Powelson, K. W., Gutenspergen, G. R., and Takekawa, J. Y., (2015), Marshes to mudflats—Effects of sea-level rise on tidal marshes along a latitudinal gradient in the Pacific Northwest: U.S. Geological Survey Open-File Report 2015-1204, 54 p. plus appendixes, http://dx.doi.org/10.3133/ofr20151204.

Thorne, K.M., MacDonald, G.M., Ambrose, R. F., Buffington, K.J., Freeman, C.M., Janousek, C.N., Brown, L.N., Holmquist, J.R., Gutenspergen, G.R., Powelson, K.W., Barnard, P.L., and Takekawa, J.Y., 2016, Effects of climate change on tidal marshes along a latitudinal gradient in California: U.S. Geological Survey Open-File Report 2016-1125, 75 p., **http://dx.doi.org/10.3133/ofr20161125**.

List of Figure Captions

Fig. 1. Location of 17 tidal marsh study sites along the Pacific coast of the United States. Study sites represented a range of dominant tidal marsh vegetation, climate, and tidal ranges to test the applicability of model corrections across different vegetation types.

Fig. 2. Boxplot of uncorrected lidar error (top) and errors from Lidar Elevation Adjustment using NDVI (LEAN) corrections (bottom) across study sites. Lidar error was calculated by subtracting RTK-GPS elevation from the lidar DEM. Box shading designates region (light grey: Pacific Northwest, white: San Francisco Bay, dark grey: Southern California). Sites are ordered from north to south.

Fig. 3. Positive bias in lidar DEM before Lidar Elevation Adjustment using NDVI (LEAN) correction (top) and after LEAN correction (bottom), with a 1:1 line. Units in m, NAVD88.

Fig. 4. Example results from each region (Pacific Northwest: Grays Harbor; San Francisco Bay: Petaluma; Southern California: Tijuana. (a) Uncorrected lidar digital terrain model (DEM; (b) model adjusted DEM, and (c) total adjustment. Elevation in m, National Vertical Datum of 1988.